Guided-Wave and Leakage Characteristics of Substrate Integrated Waveguide

Feng Xu and Ke Wu, *Fellow, IEEE*

***Abstract*—The substrate integrated waveguide (SIW) technique makes it possible that a complete circuit including planar circuitry, transitions, and rectangular waveguides are fabricated in planar form using a standard printed circuit board or other planar processing techniques. In this paper, guided wave and modes characteristics of such an SIW periodic structure are studied in detail for the first time. A numerical multimode calibration procedure is proposed and developed with a commercial software package on the basis of a full-wave finite-element method for the accurate extraction of complex propagation constants of the SIW structure. Two different lengths of the SIW are numerically simulated under multimode excitation. By means of our proposed technique, the complex propagation constant of each SIW mode can accurately be extracted and the electromagnetic bandstop phenomena of periodic structures are also investigated. Experiments are made to validate our proposed technique. Simple design rules are provided and discussed.**

***Index Terms*—Commercial electromagnetic simulator, complex modes, leakage, numerical calibration, substrate integrated waveguide (SIW).**

I. Introduction

IN MULTILAYER microwave integrated circuits such as low-temperature co-fired ceramics (LTCCs) or multilayer printed circuit boards (PCBs), waveguide-like structures can be fabricated in planar form by using periodic metallic via holes called substrate integrated waveguides (SIWs). Such SIW structures can largely preserve the well-known advantages of conventional rectangular waveguides, namely, high-Q factor and high power capacity. Integrated rectangular waveguide concepts have recently been studied and developed [1]–[6].

Judging from the periodic gaps, the SIW structures are subject to a possible leakage problem, thus potentially resulting in wave attenuation or leakage. It is, therefore, very important to investigate what type of guided-wave modes may exist along the SIW, and understand why these modes can exist, and what are the similarity and difference when the SIW has been compared with normal waveguides. Of course, it is of critical importance to obtain the propagation characteristics of complex modes and bandstop properties of the SIW structure. Such basic characteristics still remain unknown, although numerous investigations for SIW circuits have been made.

Manuscript received April 21, 2004; revised June 27, 2004. This work was supported in part by the Natural Sciences and Engineering Research Council of Canada.

The authors are with the Poly-Grames Research Center, Département de Génie Électrique, École Polytechnique de Montréal, Montréal, QC, Canada H3V 1A2 (e-mail: xuf@grmes.polymtl.ca; wuke@grmes.polymtl.ca).

Digital Object Identifier 10.1109/TMTT.2004.839303

In this paper, two numerical methods are used to analyze the SIW guided-wave mode features. The first is a finite-difference frequency-domain (FDFD) algorithm for the modeling of guided-wave properties [7]. The second is a numerical multimode calibration [8], which is developed and integrated with a commercial software package on the basis of a full-wave finite-element method (FEM).

More and more RF and microwave engineers and researchers make use of commercial electromagnetic simulators for their project research and development. However, nearly every commercial full-wave software package only provides network parameters at specified external locations along the feed line so that most commercial simulators cannot be used in the calculation of eigenvalue problems. An appropriate combination of the numerical multimode calibration technique and commercial simulator can obliterate the shortcoming in connection with the guided-wave eigenvalue problems. Although the proposed method in this paper requires more simulation time than the FDFD scheme, it actually provides a very simple, efficient, and accurate analysis method of the guided-wave problems for RF and microwave engineers and researchers. Moreover, complex propagation constant can be resolved if radiation and/or absorbing boundary conditions are involved in the simulators. The emphasis of this study is to uncover interesting SIW guided-wave properties. On the other hand, the two numerical methods are simultaneously used and compared with each other.

In our study, the Agilent High-Frequency Structure Simulator (HFSS) is chosen because the scattering matrix produced by this simulator under a multimode excitation is very suitable for integration with the proposed numerical multimode calibration technique in the analysis of SIW complex modes.

Although the SIW structures have similar properties as the conventional rectangular waveguides, the differences between them are also obvious. First, the SIW is a sort of periodic (or discrete) guided-wave structures, and it may lead to an electromagnetic bandstop phenomenon. Second, the SIW structures are subject to a potential leakage problem due to the periodic gaps. Therefore, the modes or waves traveling in the SIW circuits are different from those in the normal waveguides and there exists a certain type of leakage wave. In Section II, we will discuss whether TM modes can exist in the SIW structure and which TE modes can be preserved in it. Based on the results, a multimode excitation needed in HFSS simulation can be imposed correctly. In Section III, the numerical multimode calibration technique and the FDFD method will briefly be described. Propagation constants and cutoff frequencies will be discussed in Section IV. Attenuation constants of each mode will be mod-

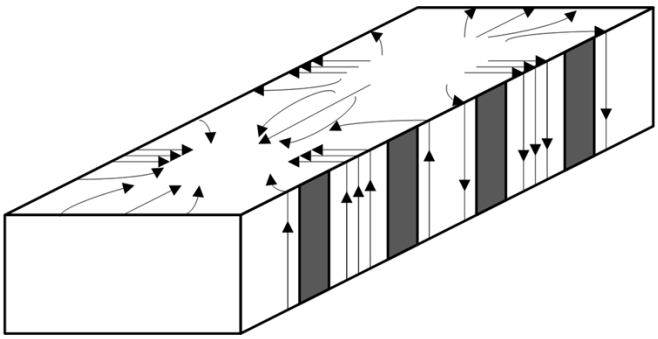

Fig. 1. TE_{10} surface currents distribution of the rectangular waveguide with slots on the narrow walls.

eled and given in Section V. Finally, we will describe the electromagnetic bandstop phenomenon of the periodic SIW structures in Section VI.

II. Modes in the SIW Structures

TM modes cannot be extracted in the SIW structures by using the FDFD method mentioned above and, moreover, only TE_{n0} modes can be excited and extracted. In other words, only TE_{n0} modes can exist in the SIW structures. This is an important feature of the structure and a clear physical explanation is needed. In fact, when a mode is established in some guided-wave structure, the surface currents are then established. The SIW structure can be regarded as a special rectangular waveguide with a series of slots on the bilateral narrow walls. If the slots cut the currents, a large amount of radiation may appear. This is the well-established design principle of waveguide slot antenna. However, if the slots are cut along the direction of current flowing, there is only very little radiation.

The TE_{10}-mode surface current flowing pattern of a rectangular waveguide with slots on its bilateral narrow walls is shown in Fig. 1. The slots do not cut the surface current on the narrow walls; the mode can thus be preserved in the structure. The other TE_{n0} modes have similar surface currents on the narrow walls. This is why TE_{n0} modes can exist in the SIW structures.

Now, let us suppose TM modes traveling in a rectangular waveguide with slots on the narrow walls; transverse magnetic field will produce a longitudinal surface current. The transverse slots cutting these currents will bring about a large amount of radiation. By the same reason, these slots will also yield a large amount of radiation if $\mathrm{TE}_{\mathrm{nm}}$ (with m not being equal to zero) modes travel in the waveguide with slots on the narrow walls. Therefore, the slot radiation suggests that only TE_{n0} modes would be allowed in the structure.

In our early research, we fabricated the SIW circuits with a mechanic process that involves drilling holes on the PCB, inserting the metal pins, and soldering them together with metal plates. We found that if the pins are not soldered together with the metal plates of PCB, S-parameter properties of the SIW will degrade in a very significant way. Thus, the metal posts not only play a role shielding the electromagnetic waves, but also are responsible for connecting the surface currents in order to preserve the guided-wave propagation. In addition, as mentioned in the beginning of this section, we can only extract the TE_{n0} guided modes when the FDFD method is used to analyze the SIW structure. We can conclude that the guided modes of the SIW are only TE_{n0} modes.

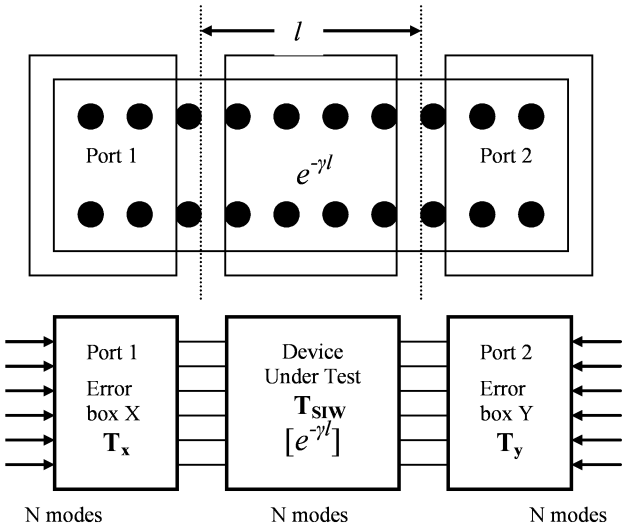

Fig. 2. Block diagram of the proposed numerical multimode calibration procedure.

III. Numerical Methods

When a multiline method is used in practice to analyze the propagation constant of a transmission line [9], a network analyzer calibration is unnecessary since calibrated scattering parameters are not required [10]. This can be extended to our multimode calibration cases [11], [12], i.e., by means of two generalized scattering matrix calculations of a line connection, we are able to calibrate and extract the propagation constant of each SIW mode.

Although the single-mode calibration technique [9], [10] can be used to analyze each SIW mode, errors will manifest at some frequencies where multimodes exist, thus leading to inaccurate results. It is thus necessary to apply the numerical multimode calibration techniques to analyze and accurately extract parametric characteristics of the SIW modes. As shown in Fig. 2, the simulated matrix $\mathbf{T}$ can be written as a cascade matrix form

$$\mathbf{T} = \mathbf{T_X}\mathbf{T_{SIW}}\mathbf{T_Y} \tag{1}$$

where $\mathbf{T_{SIW}}$ is a diagonal matrix

$$\mathbf{T_{SIW}} = \mathrm{diag}\left[e^{\gamma_1 l} \quad \cdots \quad e^{\gamma_n l} \quad e^{-\gamma_1 l} \quad \cdots \quad e^{-\gamma_n l}\right] \tag{2}$$

where γ is the propagation constant and l is the length of transmission line. The simulated cascade matrices of two transmission lines (i and j) of different length can be combined into an eigenvalue equation

$$\mathbf{T^{ij}}\mathbf{T_X} = \mathbf{T_X}\mathbf{T_{SIW}^{ij}} \tag{3}$$

where

$$\mathbf{T^{ij}} = \mathbf{T^i}(\mathbf{T^j})^{-1} \tag{4}$$

and

$$\mathbf{T_{SIW}^{ij}} = \mathbf{T_{SIW}^i}\left(\mathbf{T_{SIW}^j}\right)^{-1}. \tag{5}$$

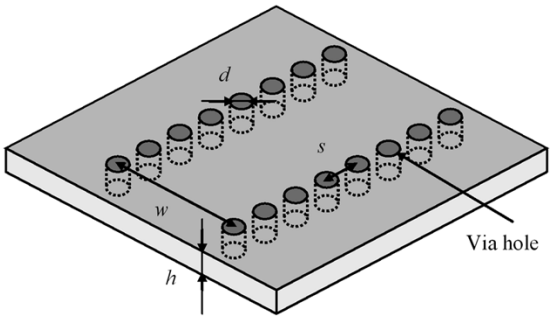

Fig. 3. Configuration of an SIW structure synthesized using metallic via-hole arrays.

Since $\mathbf{T}^{\mathbf{ij}}_{\mathbf{SIW}}$ is a diagonal matrix, the eigenvalues of $\mathbf{T}^{\mathbf{ij}}$ are simply the diagonal elements of the $\mathbf{T}^{\mathbf{ij}}_{\mathbf{SIW}}$ matrix. This is used to derive the unknown SIW propagation constants

$$e^{\gamma_i \Delta l} = \lambda_i \tag{6}$$

where λ_i is the eigenvalue of $\mathbf{T}^{\mathbf{ij}}$, and Δl is the difference of the two SIW lines of different length. Each mode is associated with two opposite propagation constants and a pair of inverse eigenvalues. Since the SIW transmission line is an open periodic structure, we can easily extract the propagation constants according to the attenuation constant of each mode.

The FDFD method we proposed and developed for modeling the guided-wave properties in [7] is an algorithm that can model periodic structures of complicated geometry and anisotropy. The computational domain is restricted to a single period. The guided-wave problem can be converted into an eigenvalue problem as follows:

$$\gamma \mathbf{B}\mathbf{x} = \mathbf{A}\mathbf{x} \tag{7}$$

where γ is a complex propagation constant. The algorithm has advantages to handle a periodic guided-wave problem quickly and accurately, however, a very tedious programming job is required.

IV. Propagation Constant and Cutoff Frequency

Fig. 3 shows a typical SIW structure that is synthesized with linear arrays of metallic via-holes on a low-loss substrate. Fig. 4 presents multimode calibration and simulation results of a TE_{10}-mode propagation constant compared with measured results, as well as calculated results based on its equivalent rectangular waveguide. As shown in Fig. 3, the sizes of the SIW are selected as $\epsilon_r = 2.33, d = 0.8$ mm, $s = 2.0$ mm, $w = 7.2$ mm, and $h = 0.508$ mm. Excellent agreement between the measured and calibrated results has verified the proposed multimode calibration method. Experiments and simulations have proven that dispersion characteristics of the SIW are the same as those of its equivalent rectangular waveguide. The equivalent width of the SIW is between w and $(w-d)$ with a very good approximate equation [5]

$$w_{\text{eff}} = w - \frac{d^2}{0.95 \cdot s} \tag{8}$$

provided that s is sufficiently small.

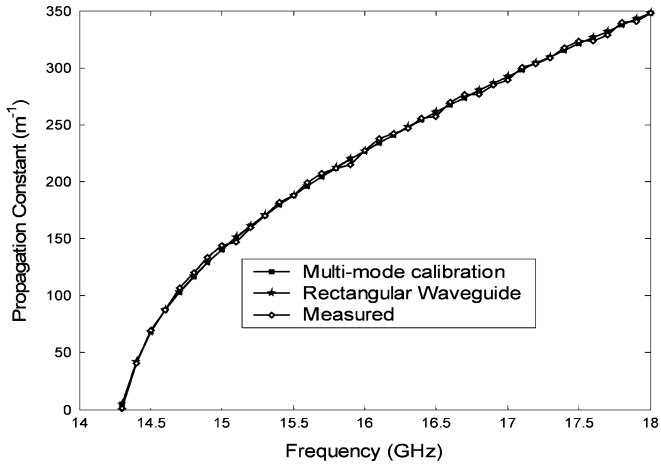

Fig. 4. Comparison of a TE_{10}-mode propagation constant between calculated results using the numerical multimode calibration method and measured results, as well as calculated results of an equivalent rectangular waveguide.

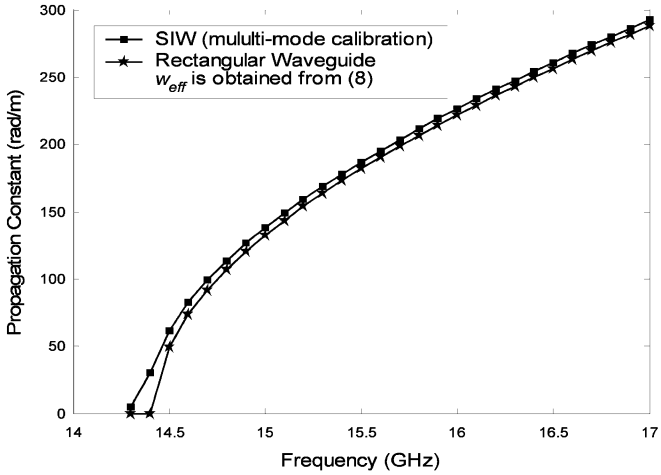

Fig. 5. Comparison of a TE_{10}-mode propagation constant between an SIW ($\epsilon_r = 2.33, d = 0.8$ mm, $s = 2.0$ mm, $w = 7.2$ mm, $h = 0.508$ mm) and an equivalent rectangular waveguide ($\epsilon_r = 2.33$) whose width w_{eff} is obtained from (8).

Actually, w_{eff} is decided by three parameters, namely, w, s, and d. However, the modified term in (8) does not include the effect of d/w. When d increases, the small error will appear, as shown in Fig. 5. A more accurate empirical equation is proposed here as follows:

$$w_{\text{eff}} = w - 1.08 \cdot \frac{d^2}{s} + 0.1 \cdot \frac{d^2}{w}. \tag{9}$$

When s/d is smaller than three and d/w is smaller than 1/5, the empirical equation is very accurate. Fig. 6 shows the comparison of propagation constants between the same SIW used as in Fig. 5 and the rectangular waveguide whose equivalent width w_{eff} is calculated from (9).

For high-order modes of the SIW, the dispersion characteristics are also the same as its equivalent rectangular counterpart. However, there is a little difference in the equivalent width w_{eff} between the high-order modes and the fundamental mode [5].

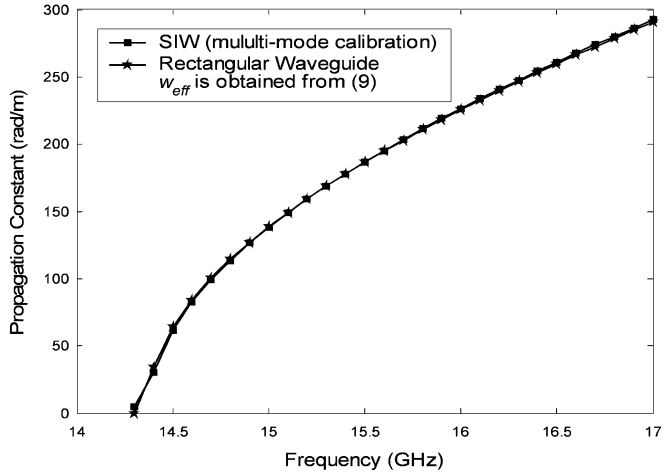

Fig. 6. Comparison of a TE_{10}-mode propagation constant between the same SIW used as in Fig. 5 and an equivalent rectangular waveguide whose width w_{eff} is obtained from (9).

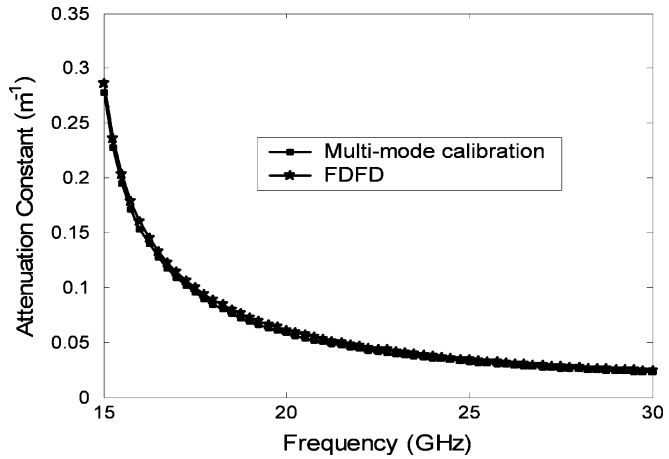

Fig. 7. TE_{10}-mode attenuation constant calculated by using the numerical multimode calibration method and FDFD method.

V. Attenuation Constant of the SIW

As mentioned earlier, the leakage of electromagnetic fields will result in wave attenuation because of the periodic gaps. With the use of absorbing boundary condition, the attenuation constant can be extracted. Figs. 7–9 depict the attenuation constant of the SIW for $\mathrm{TE}_{10}, \mathrm{TE}_{20}$, and TE_{30} modes, respectively. As shown in Fig. 3, the sizes of the SIW are selected as $\epsilon_r = 2.33, d = 0.8$ mm, $s = 2.0$ mm, $w = 7.2$ mm, and $h = 0.508$ mm. Good agreement between the two methods can be observed in these figures. From these figures, the leakage is always larger at lower frequencies and the attenuation constant increases quickly by the ascending of modes. It is apparent that these phenomena are very hard to explain. However, a good physical explanation will definitely be beneficial in understanding these phenomena.

To do so, let us review the propagation process of an electromagnetic wave in the conventional rectangular waveguide. As shown in Fig. 10, an electromagnetic wave travels in the z-direction by reflecting between two broad sidewalls (TE_{n0} modes). Looking into various modes, we have

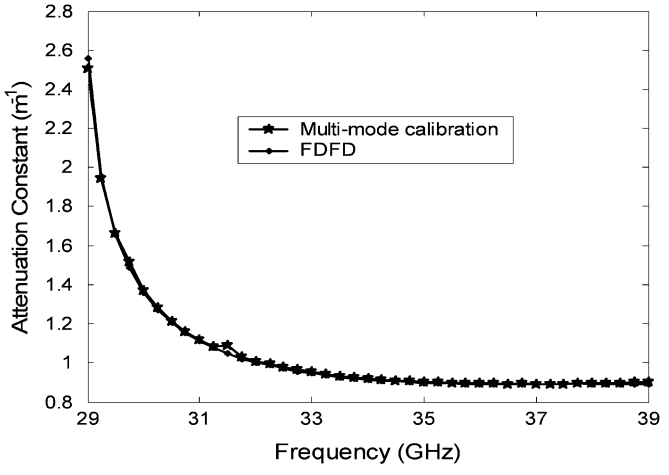

Fig. 8. TE_{20}-mode attenuation constant calculated by using the numerical multimode calibration method and FDFD method.

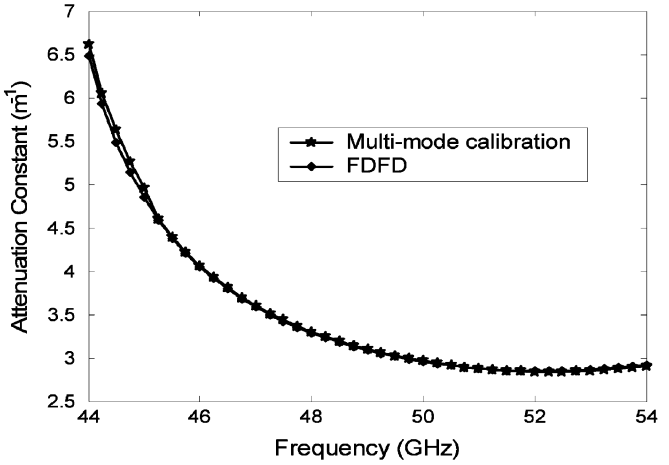

Fig. 9. TE_{30}-mode attenuation constant calculated by using the numerical multimode calibration method and FDFD method.

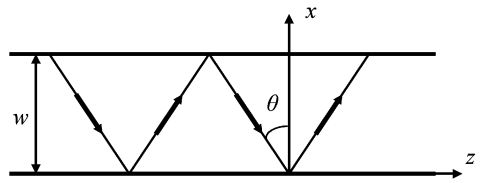

Fig. 10. Electromagnetic wave (TE_{n0} modes) traveling in waveguide.

$$\cos\theta = \frac{n\lambda}{2w} \tag{10}$$

where n represents waveguide mode order, w is the length of the broad sidewall of waveguide, and λ is the wavelength. When the wavelength decreases or frequency increases, the angle θ increases. When mode order n increases, the angle θ decreases.

As shown in Fig. 11, we can suppose that the electromagnetic wave propagates in the SIW with a similar manner as in a rectangular waveguide. The leakage part ratio can be approximately expressed by

$$R_{\mathrm{leak}} = 1 - \frac{d}{s\cos\theta}, \qquad \theta < \theta_c \tag{11}$$

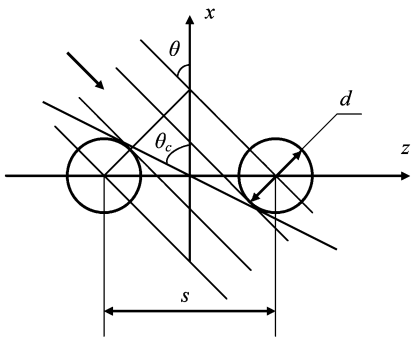

Fig. 11. Electromagnetic wave incidence to metal cylinders.

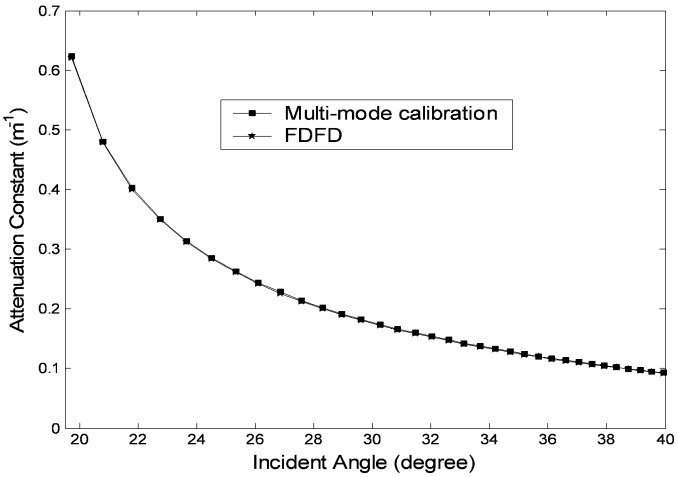

Fig. 12. TE_{10}-mode attenuation constant with respect to incident angle.

where $\cos\theta$ is approximately formulated in (10). In this manner, we can give a very clear physical explanation for the above-described characteristics of the SIW. First, when frequency increases, the leakage will increase if the incident angle remains unchanged. However, the angle θ will increase with the ascending of frequency. This leads to the decrease of R_{leak}, especially when angle θ is in the range of 15°–50°. The influence of incident angle on the attenuation constant is larger than that of frequency especially over a low frequency range. Angle θ decreases when the mode order n increases. This leads to the increase of R_{leak}, and the attenuation constant thus increases while n increases. Due to the discrete n variation, except for very small spacing s, the attenuation constant will increase in a significant manner.

We transfer characteristic parameter from frequency to incident angle according to (10), and redrawing Figs. 7–9 will generate a new set of Figs. 12–14, which give the attenuation constant of $\mathrm{TE}_{10}, \mathrm{TE}_{20}$, and TE_{30} modes with respect to the incident angle, respectively. From these figures, it is obvious that (11) can explain the cases of attenuation constants of each TE_{n0} mode. A low-frequency rather than high-frequency design rule can be suggested.

Fig. 15 shows the comparison of attenuation constants between measured results and simulated results ($\epsilon_r = 2.33, d = 0.8$ mm, $s = 2.0$ mm, $w = 7.2$ mm, $h = 0.508$ mm). Calibration techniques are used in both of them. Two SIW lines of different length are made and measured. In the range of 15–25 GHz, only TE_{10} mode exists in the SIW lines. Good agreement between the measured and calibrated results can be observed. In addition, the measured results have also verified the proposed method of the multimode

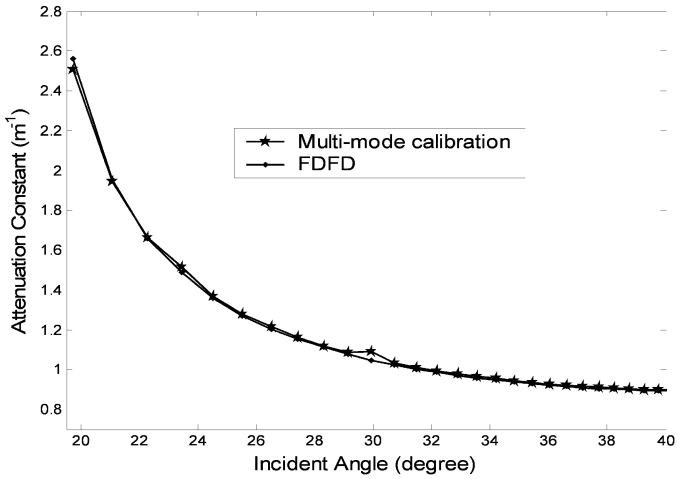

Fig. 13. TE_{20}-mode attenuation constant with respect to incident angle.

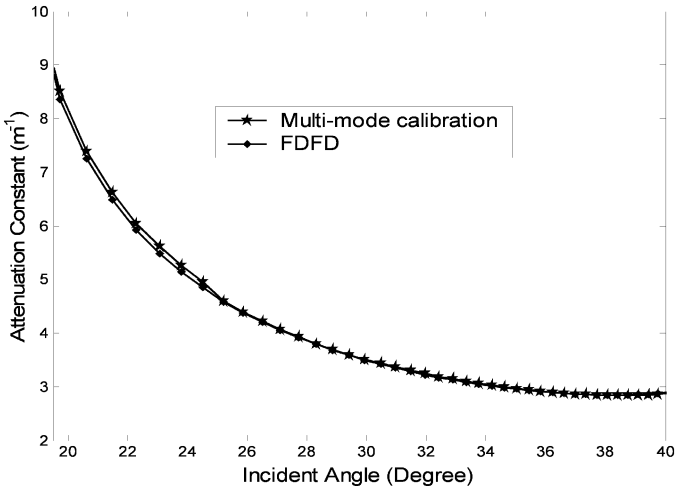

Fig. 14. TE_{30}-mode attenuation constant with respect to incident angle.

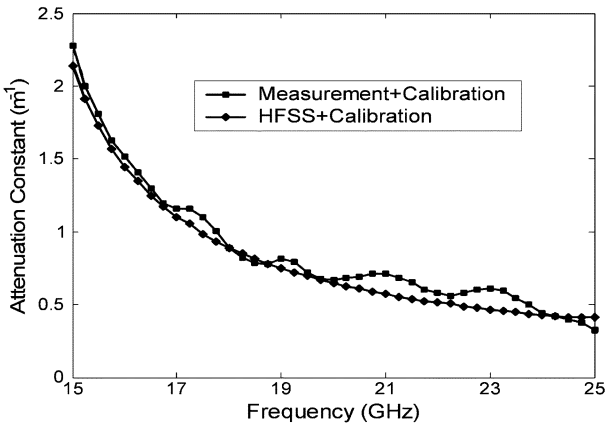

Fig. 15. Measured TE_{10}-mode attenuation constant of the SIW with the experimental calibration and HFSS simulated results with the proposed numerical calibration technique.

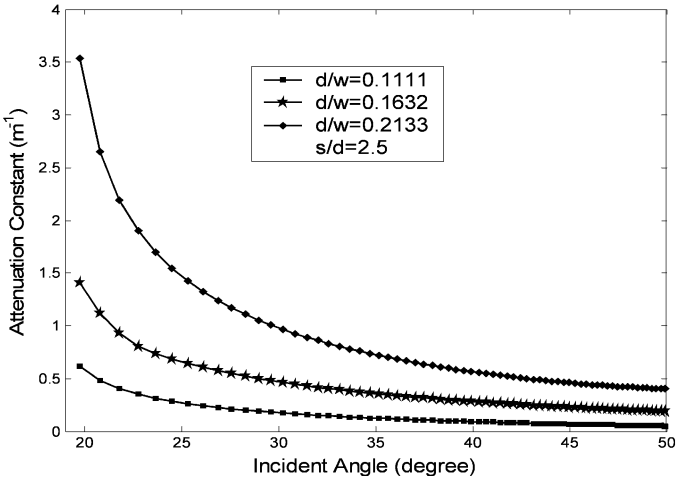

Fig. 16. Properties of the TE_{10}-mode attenuation constant (s/d remains unchanged ($s/d = 2.5$)).

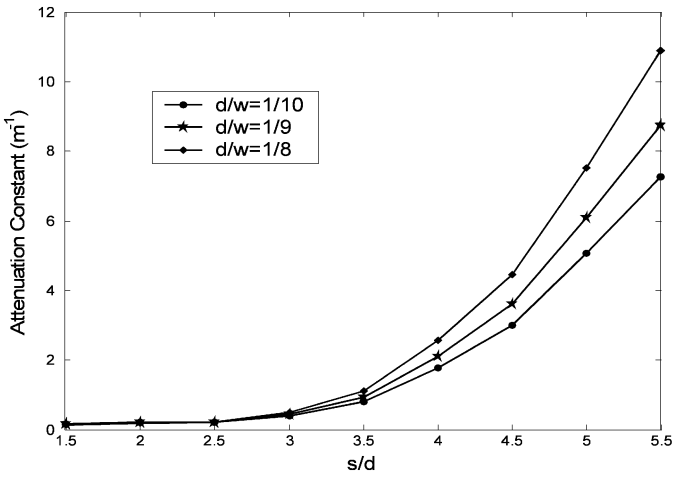

Fig. 17. Properties of the TE_{10}-mode attenuation constant (d and w_{eff} remain unchanged and the incident angle is 30°).

calibration technique integrated with simulation software (in our case, HFSS).

When d/w increases, and $s/d(= 2.5)$ and w_{eff} [from (9)] remain unchanged, a set of TE_{10} attenuation constants from the multimode calibration technique are shown in Fig. 16. From this figure, the smaller d/w is, the better loss characteristic of the SIW structure becomes if s/d remains unchanged. Fig. 17 shows the attenuation constants calculated by using the FDFD method when s/d increases gradually. All of incident angles calculated from (10) are 30°.

When the diameter d of via-posts increases, s/d should be compressed to reduce leakage loss. However, our study has demonstrated that when d/w is relatively large, larger d and smaller s will result in the degradation of SIW dispersion characteristics. Thus, the size of d/w should be as small as possible. A design rule with $s/d < 2.0$ and $d/w < 1/5$ is then recommended from our analysis. Based on this condition, the leakage loss is very small; moreover, (9) is very accurate. By means of (9), the dispersion characteristics of the SIW structure can be obtained quickly. The design procedure is as follows.

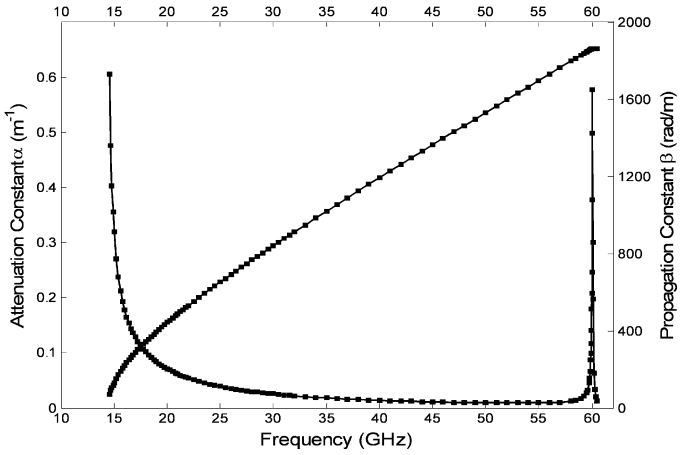

Fig. 18. TE_{10}-mode complex propagation constant calculated by using the FDFD method. SIW sizes are $d = 0.8$ mm, $s = 2.0$ mm, $w = 7.6$ mm, $\epsilon_r = 2.33, s/d = 2.5, d/w = 0.1053$.

Step 1) Select $s/d(<2.0)$.
Step 2) Select $d/w(<1/5)$.
Step 3) Calculate w_{eff} according to operating frequency.
Step 4) Calculate w by solving (9).
Step 5) Calculate d and s according to d/w and s/d.

When selecting d/w smaller than 1/8, a simpler design rule is recommended. From the tendency of the attenuation constant curve, a low-frequency design scheme is suggested. It means from (10)

$$w = \frac{c}{2f_l\sqrt{\varepsilon_r}\cos\theta} \tag{12}$$

where f_l is the lowest operating frequency. It is good to choose the angle around 30° as the critical value. The design procedure is as follows.

Step 1) Select $s/d(<2.5)$.
Step 2) Select $d/w(<1/8)$.
Step 3) Select an incident angle equal to or larger than 30°, and then calculate w from (12).
Step 4) Calculate d and s according to d/w and s/d.

Due to some technical reasons, e.g., limited manufacturing techniques, d/w has to be larger than 1/5. It is then better to use a numerical technique, e.g., two methods used in this paper, to calculate an accurate complex propagation constant. When d/w increases, a smaller s/d is needed.

VI. Bandstop Phenomenon of the SIW

Since the SIW is a periodic guided-wave structure, the electromagnetic bandstop phenomena will probably appear. Fig. 18 shows the complex propagation constant of an SIW TE_{10} mode ($d = 0.8$ mm, $s = 2.0$ mm, $w = 7.6$ mm, $\epsilon_r = 2.33, s/d = 2.5, d/w = 0.1053$), which is obtained by using the FDFD method. Increasing s to 2.8 mm ($s/d = 3.5$), the complex propagation constant of the SIW TE_{10} mode is shown in Fig. 19. In addition, two numerical methods are used in Fig. 19 to compare the results between them. Fig. 20 shows the complex propagation constant of another SIW whose parameter d/w increases and parameter s/d remains as 2.5 ($d = 1.2$ mm, $s = 3.0$ mm, $w = 7.8$ mm, $\epsilon_r = 2.33, s/d = 2.5, d/w = 0.1538$). From

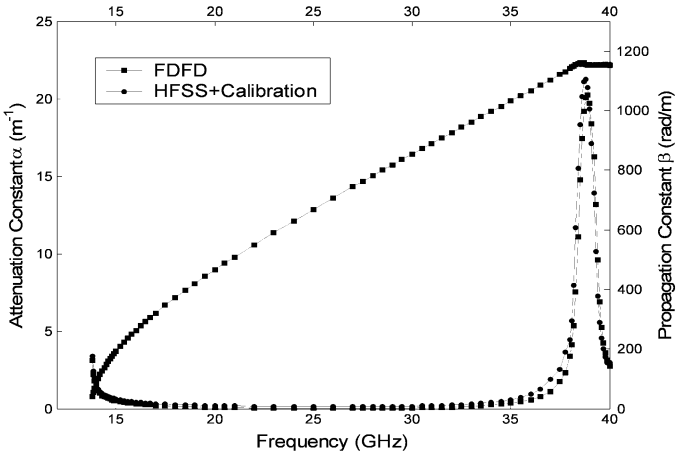

Fig. 19. TE_{10}-mode complex propagation constant calculated by using the FDFD method. SIW sizes are $d = 0.8$ mm, $s = 2.8$ mm, $w = 7.6$ mm, $\epsilon_r = 2.33, s/d = 3.5, d/w = 0.1053$.

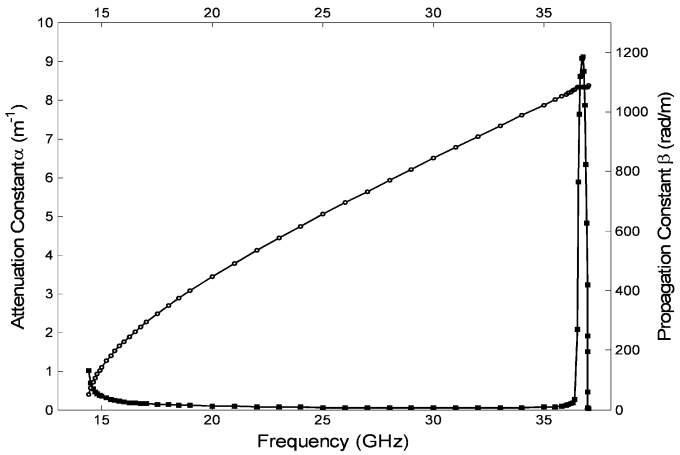

Fig. 20. TE_{10}-mode complex propagation constant calculated by using the FDFD method. SIW sizes are $d = 1.2$ mm, $s = 3.0$ mm, $w = 7.8$ mm, $\epsilon_r = 2.33, s/d = 2.5, d/w = 0.1538$.

these figures, the frequency where bandstop appears is also very high if s/d and d/w are small, and also the bandstop width and magnitude are very small. When d/w or s/d increases, the width and magnitude of bandstop will become significantly large, and the frequency point at which the bandstop appears will largely move to lower frequency.

VII. Conclusion

A numerical multimode calibration technique has been presented and integrated with a commercial simulator for the analysis of guided-wave properties of an SIW transmission line. Our comparative investigation has demonstrated that only TE_{n0} modes can exist in the SIW structures and the SIW transmission lines have the similar dispersion characteristics as in a rectangular waveguide for TE_{n0} modes. Small posts and small spacing between via-posts are not only beneficial to dispersion characteristics, leakage loss, and bandstop properties of the SIW structure, but also greatly simplify the design procedure and make the PCB design much more compact.

Acknowledgment

The authors wish to acknowledge the technical assistance and support of J. Xu, Poly-Grames Research Center, École Polytechnique de Montréal, Montréal, QC, Canada, for the experiments.

References

[1] J. Hirokawa and M. Ando, "Single-layer feed waveguide consisting of posts for plane TEM wave excitation in parallel plates," *IEEE Trans. Antennas Propag.*, vol. 46, no. 5, pp. 625–630, May 1998.

[2] D. Deslandes and K. Wu, "Integrated transition of coplanar to rectangular waveguides," in *IEEE MTT-S Int. Microwave Symp. Dig.*, Feb. 2001, pp. 619–622.

[3] ——, "Integrated microstrip and rectangular waveguide in planar form," *IEEE Microwave Wireless Compon. Lett.*, vol. 11, no. 2, pp. 68–70, Feb. 2001.

[4] A. Zeid and H. Baudrand, "Electromagnetic scattering by metallic holes and its applications in microwave circuit design," *IEEE Trans. Microw. Theory Tech.*, vol. 50, no. 4, pp. 1198–1206, Apr. 2002.

[5] Y. Cassivi, L. Perregrini, P. Arcioni, M. Bressan, K. Wu, and G. Conciauro, "Dispersion characteristics of substrate integrated rectangular waveguide," in *IEEE Microwave Wireless Compon. Lett.*, vol. 12, Sep. 2002, pp. 333–335.

[6] D. Deslande and K. Wu, "Single-substrate integration technique of planar circuits and waveguide filters," *IEEE Trans. Microw. Theory Tech.*, vol. 51, no. 2, pp. 593–596, Feb. 2003.

[7] F. Xu, Y. Zhang, W. Hong, K. Wu, and T. J. Cui, "Finite-difference frequency-domain algorithm for modeling guided-wave properties of substrate integrated waveguide," *IEEE Trans. Microw. Theory Tech.*, vol. 51, no. 11, pp. 2221–2227, Nov. 2003.

[8] F. Xu and K. Wu, "Numerical multimode calibration technique for extraction of complex propagation constants of substrate integrated waveguide," in *IEEE MTT-S Int. Microwave Symp. Dig.*, 2004, pp. 1227–1230.

[9] R. Marks, "A multiline method of network analyzer calibration," *IEEE Trans. Microw. Theory Tech.*, vol. 39, pp. 1205–1215, Jul. 1991.

[10] M. D. Janezic and J. A. Jargon, "Complex permittivity determination from propagation constant measurements," *IEEE Microw. Guided Wave Lett.*, vol. 9, no. 2, pp. 76–78, Feb. 1999.

[11] H. W. Glock and U. van Rienen, "An iterative algorithm to evaluate multimodal S-parameter-measurements," *IEEE Trans. Magn.*, vol. 36, no. 4, pp. 1841–1845, Jul. 2000.

[12] C. Seguinot, P. Kennis, J. F. Legier, F. Huret, E. Paleczny, and L. Hayden, "Multimode TRL—A new concept in microwave measurements: Theory and experimental verification," *IEEE Trans. Microw. Theory Tech.*, vol. 46, no. 5, pp. 536–542, May 1998.

[13] L. Zhu and K. Wu, "Unified equivalent-circuit model of planar discontinuities suitable for field theory-based CAD and optimization of M(H)MIC's," *IEEE Trans. Microw. Theory Tech.*, vol. 47, pp. 1589–1602, Sep. 1999.

Feng Xu was born in Jiangsu, China. He received the B.S. degree in radio engineering from Southeast University, Nanjing, China, in 1985, the M.S. degree in microwave and millimeter-wave theory and technology from the Nanjing Research Institute of Electronics and Technology, Nanjing, China, in 1998, and the Ph.D. degree in radio engineering from Southeast University, Nanjing, China, in 2002.

From 1985 to 1996, he was with the Nanjing Research Institute of Electronics and Technology, where he conducted research in the areas of antenna and RF circuits design. Since 2002, he has been a Post-Doctoral Researcher with the Poly-Grames Research Center, Département de Génie Électrique, École Polytechnique de Montréal, Montréal, Canada. His current research interests include numerical methods for electromagnetic field problem, and advanced microwave and millimeter-wave circuits and components.

Ke Wu (M'87–SM'92–F'01) was born in Liyang, Jiangsu Province, China. He received the B.Sc. degree (with distinction) in radio engineering from the Nanjing Institute of Technology (now Southeast University), Nanjing, China, in 1982, and the D.E.A. and Ph.D. degrees in optics, optoelectronics, and microwave engineering (with distinction) from the Institut National Polytechnique de Grenoble (INPG), Grenoble, France, in 1984 and 1987, respectively.

He conducted research with the Department of Electrical and Computer Engineering, University of Victoria, Victoria, BC, Canada, prior to joining the École Polytechnique de Montréal (Engineering School affiliated with the University of Montreal), Montréal, QC, Canada, as an Assistant Professor. He is currently a Professor of Electrical Engineering, and Canada Research Chair in Radio-Frequency and Millimeter-Wave Engineering. He has been a Visiting or Guest Professor with the Telecom-Paris, Paris, France, INPG, the City University of Hong Kong, Hong Kong, the Swiss Federal Institute of Technology (ETH-Zurich), Zurich, Switzerland, the National University of Singapore, Singapore, the University of Ulm, Ulm, Germany, and the Technical University Munich, Munich, Germany, as well as many short-term visiting professorships with other universities. He also holds an honorary visiting professorship and a Cheung Kong endowed chair professorship (visiting) with Southeast University, Nanjing, China, and an honorary professorship with the Nanjing University of Science and Technology, Nanjing, China. He has been the Director of the Poly-Grames Research Center, as well as the Founding Director of the Canadian Facility for Advanced Millimeter-Wave Engineering (FAME). He has authored or coauthored over 370 referred papers and also several books/book chapters. His current research interests involve hybrid/monolithic planar and nonplanar integration techniques, active and passive circuits, antenna arrays, advanced field-theory-based computer-aided design (CAD) and modeling techniques, and development of low-cost RF and millimeter-wave transceivers. He is also interested in the modeling and design of microwave photonic circuits and systems. He serves on the Editorial Board of *Microwave and Optical Technology Letters*, the *International Journal of RF and Microwave Computer-Aided Engineering* (RFMiCAE), and Wiley's *Encyclopedia of RF and Microwave Engineering*.

Dr. Wu is a member of the Electromagnetics Academy, the Sigma Xi Honorary Society, and the URSI. He is a Fellow of the Canadian Academy of Engineering (CAE). He has held numerous positions in and has served on various international committees, including the vice-chairperson of the Technical Program Committee (TPC) for the 1997 Asia–Pacific Microwave Conference, the general cochair of the 1999 and 2000 SPIE International Symposium on Terahertz and Gigahertz Electronics and Photonics, the general chair of the 8th International Microwave and Optical Technology (ISMOT'2001), the TPC chair of the 2003 IEEE Radio and Wireless Conference (RAWCON'2003), the general co-chair of the 2004 IEEE Radio and Wireless Conference (RAWCON'2004). He has served on the Editorial or Review Boards of various technical journals, including the IEEE TRANSACTIONS ON MICROWAVE THEORY AND TECHNIQUES, the IEEE TRANSACTIONS ON ANTENNAS AND PROPAGATION, and the IEEE MICROWAVE AND WIRELESS COMPONENTS LETTERS. He served on the 1996 IEEE Admission and Advancement Committee and the Steering Committee for the 1997 joint IEEE Antennas and Propagation Society (AP-S)/URSI International Symposium. He has also served as a TPC member for the IEEE Microwave Theory and Techniques Society (IEEE MTT-S) International Microwave Symposium (IMS). He was elected into the Board of Directors of the Canadian Institute for Telecommunication Research (CITR). He served on the Technical Advisory Board of Lumenon Lightwave Technology Inc. He is currently the chair of the joint chapters of the IEEE MTT-S/AP-S/LEOS in Montreal, QC, Canada, and the chapter coordinator for IEEE MTT-S Region 7. He was the recipient of a URSI Young Scientist Award, the Oliver Lodge Premium Award of the Institute of Electrical Engineer (IEE), U.K., the Asia–Pacific Microwave Prize, the University Research Award "Prix Poly 1873 pour l'Excellence en Recherche" presented by the École Polytechnique de Montréal on the occasion of its 125th anniversary, and the Urgel-Archambault Prize (the highest honor) in the field of physical sciences, mathematics, and engineering from the French–Canadian Association for the Advancement of Science (ACFAS). In 2002, he was the first recipient of the IEEE MTT-S Outstanding Young Engineer Award.